Chen, C., Liu, W., Lin, C.-H., and Chen, Q. 2015. "Comparing the Markov chain model with the Eulerian and Lagrangian models for indoor transient particle transport simulation." *Aerosol Science & Technology*, 49, 857-871.

Comparing the Markov Chain Model with the Eulerian and Lagrangian Models for Indoor Transient Particle Transport Simulations

Chun Chen[1], Wei Liu[3,1], Chao-Hsin Lin[2], and Qingyan Chen[1,3*]

[1] School of Mechanical Engineering, Purdue University, West Lafayette, IN 47907, USA
[2] Environmental Control Systems, Boeing Commercial Airplanes, Everett, WA 98203, USA
[3] Tianjin Key Laboratory of Indoor Air Environmental Quality Control, School of Environmental Science and Engineering, Tianjin University, Tianjin 300072, China
[*] Phone: (765) 496-7562, Fax: (765) 496-0539, Email: yanchen@purdue.edu

Abstract

Correctly predicting transient particle transport in indoor environments is crucial to improving the design of ventilation systems and reducing the risk of acquiring airborne infectious diseases. Recently, a new model was developed on the basis of Markov chain frame for quickly predicting transient particle transport indoors. To evaluate this Markov chain model, this study compared it with the traditional Eulerian and Lagrangian models in terms of performance, computing cost, and robustness. Four cases of particle transport, three of which included experimental data, were used for this comparison. The Markov chain model was able to predict transient particle transport indoors with similar accuracy to the Eulerian and Lagrangian models. Furthermore, when the same time step size (Courant number $\leqslant$ 1) and grid number were used for all three models, the Markov chain model had the highest calculation speed. The Eulerian model was faster than the Lagrangian model unless a super-fine grid was used. This investigation developed empirical equations for evaluating the three models in terms of computing cost. In addition, the Markov chain model was found to be sensitive to the time step size when the Courant number is larger than 1, whereas the Eulerian and Lagrangian models were not.

Keywords: Indoor environment; Computational fluid dynamics (CFD); Aerosol; Indoor air quality; Unsteady-state.

Running Title: Comparing Three Models for Particle Transport

Nomenclature

Markov chain model	
$A_{i,nb}$ (m^2)	Area of the connecting face between cell i and the neighboring cell
$C_{k,i}$ (#/m^3)	Particle number concentration in cell i at time k
$C_{single}(t\text{-}t_i)$ (#/m^3)	Particle concentration at time $t\text{-}t_i$ because of the single pulsed source that started at time t_i
k_i (m^2/s^2)	Turbulent kinetic energy in cell i
$N_{k,i}$ (#)	Particle number in cell i at time k
$N_{k,nb}$ (#)	Particle number in the neighboring cell at time k
$p_{i,i}$	Probability of a particle's staying in cell i in a time step
$p_{i,j}$	Probability of a particle's moving from cell i to cell j in a time step
$p_{nb,i}$	Probability of a particle's moving from the neighboring cells or

	boundaries to cell i in a time step
$Q_{i,j}$ (m^3/s)	Airflow rate from cell i to cell j
$Q_{i,nb}$ (m^3/s)	Airflow rate from cell i to a neighboring cell
$Q_{mean,i,nb}$ (m^3/s)	Mean airflow rate from cell i to a neighboring cell
$Q_{fluctuating,i,nb}$ (m^3/s)	Turbulent fluctuating airflow rate from cell i to a neighboring cell
V_i (m^3)	Volume of the cell i
$\alpha_{i,nb}$	Coefficient for calculating turbulent fluctuating airflow rate
Δt (s)	Time step size
$\Delta s_{i,nb}$ (m)	Distance between the centroid of cell i and that of the neighboring cell
Eulerian model	
C ($\#/m^3$)	Particle number concentration
C_c	Cunningham coefficient caused by slippage
d_p (m)	Particle diameter
g_j (m/s^2)	Gravitational acceleration
S_c ($\#/(m^3 s)$)	Particle source term
u_j (m/s)	Averaged air velocity
u_{sj} (m/s)	Particle gravitational settling velocity
x_j (m)	Spatial axis
σ_c	Turbulent Schimit number
υ_t (m^2/s)	Turbulent kinetic viscosity
τ_p (s)	Particle relaxation time
ρ_p (kg/m^3)	Particle density
μ ($N\ s/m^2$)	Dynamic viscosity of air
λ (m)	Mean free path of air molecules
Lagrangian model	
C_D	Drag coefficient
d_p (m)	Particle diameter
$\vec{F}_a$ (m/s^2)	Brownian motion force
F_D (1/s)	Drag force coefficient
$\vec{g}$ (m/s^2)	Gravitational acceleration vector
k_i (m^2/s^2)	Turbulent kinetic energy in cell i
N_{nec} (#)	Necessary particle number in the Lagrangian model
$N_{nec,sup}$ (#)	Necessary particle number in the combined Lagrangian and superimposition method
N_{target}^* (#)	Necessary particle number in the target zone
Q (m^3/s)	Airflow rate from the inlet
Re	Reynolds number
t_s (s)	Particle source duration
$\vec{u}_a$ (m/s)	Air velocity vector
$\vec{u}_p$ (m/s)	Particle velocity vector
u_i (m/s)	Turbulent fluctuating velocity
V_{room} (m^3)	Volume of the room
V_{target} (m^3)	Volume of the target zone
ρ_p (kg/m^3)	Particle density
ρ_a (kg/m^3)	Air density
μ_α ($N\ s/m^2$)	Dynamic viscosity of air

ζ_i	Normal random number
α	Coefficient that depends on the tolerance of error
τ (s)	Room time constant

1. Introduction

The transmission of airborne infectious diseases, such as influenza (Moser et al., 1979), tuberculosis (Menzies et al., 2000), and severe acute respiratory syndrome (SARS) (Olsen et al., 2003), has become a major public concern in recent decades (Li et al., 2007). Exhalation activities by an infected person, such as breathing, coughing, and sneezing, can generate particles carrying infectious viruses (Nicas et al., 2005). These particles can be transported through indoor air and inhaled by other persons (Morawska, 2006). This process is transient in nature. Therefore, in order to improve the design of air distribution and reduce the risk of infection it is important to predict the transient particle transport in indoor environments.

Computational fluid dynamics (CFD) is a popular tool for modeling transient particle transport in enclosed environments, which consists of airflow and particle modeling. For particle modeling, the Eulerian and Lagrangian methods have been widely used. The Eulerian method treats the particle phase as a continuum and solves the scalar transport equation. For instance, Li et al. (2011) used an Eulerian model to study the spatial distribution of exhaled droplet residuals under different ventilation modes. Seepana and Lai (2012) investigated person-to-person exposure due to sneezing in a full-scale chamber with an Eulerian model. Li et al. (2012) and Chen et al. (2014) applied an Eulerian model to assess the effectiveness of covering a cough in reducing exposure to the coughed particles. Hang et al. (2014) studied the effect of human walking on interpersonal exposure to exhaled contaminants in an isolation room using an Eulerian model.

Instead of assuming particles to be a continuum, the Lagrangian model calculates the trajectories of numerous individual particles on the basis of Newton's law. For example, Chao and Wan (2006) and Gao and Niu (2007) used a Lagrangian model to investigate the dispersion of particles in a room with different ventilation modes. Gupta et al. (2011a) investigated the dispersion of exhaled droplets in a section of an aircraft cabin with the Lagrangian method. Gao et al. (2012) applied a Lagrangian model to study the lock-up phenomenon of exhaled droplets in a room with displacement ventilation. Zhang and Li (2012) studied the transport of exhaled droplets in a fully occupied high-speed rail cabin using a Lagrangian model.

Although both the Eulerian and Lagrangian models can provide detailed information about transient particle concentration distributions, they are considerably time-consuming (Wang et al., 2012). Recently, Chen et al. (2015a) developed a new model based on a Markov chain frame for predicting transient particle transport indoors. When solving the particle transport equations, the Markov chain model does not require iterations in each time step. Note that the term "iterations" throughout this paper refers only to the iterations needed for solving the partial differential equation for governing the particle transport. Thus, it has the potential to significantly reduce the computing cost. For instance, in the calculation of person-to-person particle transport in a ventilated room, the Markov chain model increased the speed of calculation by 6.3 and 8.0 times, respectively, as compared with the Eulerian and Lagrangian models (Chen et al., 2015a). Since the Markov chain model has the potential to reduce the computing cost, it is worthwhile to systematically evaluate this model in terms of performance, computing cost, and robustness.

This paper reports our effort in comparing the Markov chain model with the Eulerian and Lagrangian models for indoor transient particle transport simulations in terms of performance, computing cost, and robustness. This investigation focuses on accumulation mode particles whose deposition, resuspension, evaporation, biological and chemical reaction are negligible. These assumptions are reasonable for exhaled particles with an aerodynamic diameter from 0.1 to 3 μm (Zhao et al., 2009; Chen and Zhao, 2010; Zhu et al., 2012). On the basis of this comparison, the advantages and disadvantages of using the Markov chain model for predicting transient particle transport indoors can be identified.

2. Methods

2.1 Airflow and turbulence model

This study used the renormalization group (RNG) k-ε model (Choudhury, 1993) to calculate the airflow field in indoor spaces. This model has been recommended by Chen (1995), Zhang et al. (2007), Wang and Chen (2009) as having a good overall performance among all Reynolds-averaged Navier-Stokes (RANS) models for enclosed environments. The airflow field was calculated using ANSYS Fluent 12.1 software.

To isolate the impact of unsteady-state airflow, all the cases studied in this paper were assumed to have a steady-state airflow field, while the particle transport was transient. In reality, the airflow pattern in an indoor space is quasi-steady. However, when there is a disturbance such as an occupant's coughing or sneezing the occupant would normally cover his or her mouth, and thus the impact on the airflow pattern would be small (Chen et al., 2014). Of course, such an assumption cannot be applied to a major disturbance such as occupants' moving around.

2.2 Markov chain model

The Markov chain model applies the first-order homogeneous Markov chain technique (Ross, 1996) to the prediction of transient particle transport. If the CFD grid has n-1 cells, the additional cell n can be assigned as the space to which particles are removed. A particle number vector is assumed at the present time (state k):

$$N_k = \left(N_{k,1}\ N_{k,2} \cdots N_{k,n} \right) \tag{1}$$

where $N_{k,i}$ represents the particle number in cell i at time k. Then the number of particles in cell i after one time step (time k+1) can be expressed as (Chen et al., 2015a):

$$N_{k+1,i} = N_{k,i} p_{i,i} + \sum_{nb} N_{k,nb} p_{nb,i} \tag{2}$$

where $p_{i,i}$ is the probability of a particle's staying in cell i in a time step, Δt, and $p_{nb,i}$ is the probability of a particle's moving from the neighboring cells or boundaries to cell i in a time step. The particle number concentration in cell i at time k can be calculated by:

$$C_{k,i} = \frac{N_{k,i}}{V_i} \tag{3}$$

where V_i is the cell volume.

The transition probability of a particle staying in cell i in a time step, $p_{i,i}$, can be expressed as (Chen et al., 2015a):

$$p_{i,i} = \exp(-\sum_{nb} \frac{Q_{i,nb}}{V_i} \Delta t) \tag{4}$$

where $Q_{i,nb}$ is the airflow rate from cell i to a neighboring cell. This equation was derived from the particle mass balance equation for cell i, and its resulting exponential decay in particle concentration of this cell. The detailed derivation can be found in Chen et al. (2015a).

Assuming that cell j is one of the neighboring cells, the probability of a particle's moving from cell i to cell j in Δt can be calculated by (Chen et al., 2015a):

$$p_{i,j} = \frac{Q_{i,j}}{\sum_{nb} Q_{i,nb}} (1 - p_{i,i}) \tag{5}$$

where $Q_{i,nb}$ consists of two parts, the mean airflow rate ($Q_{mean,i,nb}$) and the turbulent fluctuating airflow rate ($Q_{fluctuating,i,nb}$):

$$Q_{i,nb} = Q_{mean,i,nb} + Q_{fluctuating,i,nb} \tag{6}$$

The mean airflow rate, $Q_{mean,i,nb}$, is obtained directly from the CFD simulation results. The turbulent fluctuating airflow rate, $Q_{fluctuating,i,nb}$, can be calculated by (Chen et al., 2015a):

$$Q_{fluctuating,i,nb} = \alpha_{i,nb} \sqrt{2k_i / 3} \cdot A_{i,nb} \tag{7}$$

where $A_{i,nb}$ is the area of the connecting face between cell i and the neighboring cell, k_i is the turbulent kinetic energy in cell i, and the coefficient $\alpha_{i,nb}$ is expressed as (Chen et al., 2015a):

$$\alpha_{i,nb} = 2 \cdot (1 - \Phi(\frac{\Delta s_{i,nb} / \Delta t}{\sqrt{2k_i / 3}})) \tag{8}$$

where $\Delta s_{i,nb}$ is the distance between the centroid of cell i and that of the neighboring cell. The cumulative distribution function of a standard normal distribution, $\phi(x)$, is:

$$\Phi(x) = \frac{1}{2}(1 + erf(\frac{x}{\sqrt{2}})) \tag{9}$$

where erf() is the error function. This study implemented a user-defined function in ANSYS Fluent 12.1 to realize the Markov chain model. It can be seen that, when solving the particle equation, the Markov chain model does not require iterations in each time step. Thus, it has the potential to reduce the computing cost. This study first used the Markov chain model to calculate the transient particle transport from a single pulsed source. Next, the

superimposition method was used to convert the transient particle concentration distributions from a single pulsed source to a distribution from an ordinary source using the following equation (Chen et al., 2015a):

$$C(t) = \sum_{for\ all\ i} C_{\text{single}}(t - t_i) \tag{10}$$

where $C_{single}(t\text{-}t_i)$ is the particle concentration at time $t\text{-}t_i$ because of the single pulsed source that started at time t_i. Note that this study used the first-order homogeneous Markov chain model.

2.3 Eulerian model

The Eulerian model solves the particle governing equation:

$$\frac{\partial[(u_j + u_{sj})C]}{\partial x_j} = \frac{\partial}{\partial x_j} \cdot (\frac{\upsilon_t}{\sigma_C} \frac{\partial C}{\partial x_j}) + S_C \tag{11}$$

where u_j is the averaged air velocity, υ_t is the turbulent viscosity, σ_c is the turbulent Schimdt number, and S_c is the particle source term. The particle gravitational settling velocity, u_{sj}, can be calculated by:

$$u_{sj} = \tau_p g_j \tag{12}$$

where τ_p is the particle relaxation time, and g_j is the gravitational acceleration. The τ_p can be expressed as:

$$\tau_{\text{p}} = \frac{\text{C}_{\text{c}} \rho_{\text{p}} d_{\text{p}}{}^2}{18\mu} \tag{13}$$

where C_c is the Cunningham coefficient caused by slippage, ρ_p is the particle density, d_p is the particle diameter, and μ is the dynamic viscosity of air. The C_c can be calculated by (Hinds, 1999):

$$\text{C}_{\text{c}} = 1 + \frac{\lambda}{d_p}(2.514 + 0.8 \times \exp(-0.55 \frac{d_p}{\lambda})) \tag{14}$$

where λ is the mean free path of air molecules. This study implemented a user-defined function in ANSYS Fluent 12.1 to realize the Eulerian model. The implicit time discretization method was adopted for the Eulerian model because it could provide more accurate results than the explicit discretization method (ANSYS, 2010).

2.4 Lagrangian model

The Lagrangian model calculates the trajectory of an individual particle using the particle momentum equation:

$$\frac{d\vec{u}_p}{dt} = F_D(\vec{u}_a - \vec{u}_p) + \frac{\vec{g}(\rho_p - \rho_a)}{\rho_p} + \vec{F}_a \quad (15)$$

where $\vec{u}_p$ is the particle velocity vector; $\vec{u}_a$ is the air velocity vector; $\vec{g}$ is the gravitational acceleration vector; ρ_p and ρ_a are the density of the particle and air, respectively; and $\vec{F}_a$ is the Brownian motion force. The drag force, $F_D(\vec{u}_a - \vec{u}_p)$, can be calculated by:

$$F_D(\vec{u}_a - \vec{u}_p) = \frac{18\mu_a}{\rho_p d_p^2}\frac{C_D \,\mathrm{Re}}{24}(\vec{u}_a - \vec{u}_p) \quad (16)$$

where μ_α is the air viscosity, d_p is the particle diameter, Re is the Reynolds number, and C_D is the drag coefficient (Morsi and Alexander, 1972).

The turbulence dispersion is modeled using the discrete random walk (DRW) model (Aliabadi and Rogak, 2011):

$$u'_i = \zeta_i \sqrt{2k_i/3} \quad (17)$$

where ζ_i is a normal random number and k_i is the turbulent kinetic energy in cell i. The particle trajectories were calculated using ANSYS Fluent 12.1 software. To convert the Lagrangian trajectories to particle number concentrations, this study implemented a user-defined function in the software. The implicit time discretization method was used for the Lagrangian model as it could provide more accurate results than the explicit discretization method (ANASYS, 2010).

The number of particles injected from the source is an input to the Lagrangian model. Statistically speaking, a large number of particles are needed in the calculations in order to ensure accuracy. For a case in which particles are emitted through an inlet or by an indoor source, the necessary particle number in the Lagrangian model can be estimated by (Chen et al., 2015b):

$$N_{nec} = \frac{\frac{t_s}{\tau}V_{\text{room}}}{\alpha(1-\exp(-\frac{t_s}{\tau}))V_{\text{target}}}N_{\text{target}}^{*} \quad (18)$$

where t_s is the particle source duration; V_{room} is the volume of the room; α is a coefficient that depends on the tolerance of error, which can be set at 1% (Chen et al., 2015b); and V_{target} is the volume of the target zone. For cases of person-to-person particle transport, the target zone can be defined as the breathing zone, whose volume is about 0.027 m^3 (OSHA, 2014). N_{target}^{*} is the necessary particle number in the target zone, which can be set at 30 (Student, 1908; Chen et al., 2015b). The parameter τ is the time constant of the room:

$$\tau = \frac{V_{\text{room}}}{Q} \quad (19)$$

where Q is the airflow rate from the inlet.

To reduce the necessary particle number and increase the speed of calculation, Chen et al. (2015b) have proposed a combined Lagrangian and superimposition method. Instead of injecting particles in each time step, as in the pure Lagrangian method, the combined Lagrangian and superimposition method injects particles only in one time step. Next, Lagrangian particle tracking is used to calculate the transient particle concentrations from this single pulsed source. Finally, the total particle concentration is calculated by superimposing the calculated particle concentrations with a time shift using Eq. (10).

The necessary particle number in the combined Lagrangian and superimposition method can be estimated by (Chen et al., 2015b):

$$N_{nec,\mathrm{sup}} = \frac{V_{\mathrm{room}}}{\alpha \cdot V_{\mathrm{target}}} N_{\mathrm{target}}{}^{*} \tag{20}$$

The combined Lagrangian and superimposition method can provide very similar results to those of the pure Lagrangian method with a lower computing cost (Gupta et al., 2011b; Chen et al., 2015b). Therefore, the combined method was used for the simulations in the present study.

3. Comparison of accuracy for the three models

This study used four cases of particle transport to assess the performance of the Markov chain model by comparing it with the Eulerian and Lagrangian models. The first case was that of particle transport from a single pulsed source in an empty chamber, from Wang and Chen (2009). The present investigation used the first case to qualitatively compare the transient particle concentration distributions predicted by the three models. The second case was particle transport in an isothermal ventilated chamber with a source at the inlet, from Zhang et al. (2009). The third case was particle transport from a source located inside a chamber with displacement ventilation, from Bolster and Linden (2009). The present study used the second and third cases to quantitatively assess the performance of the Markov chain model by comparing with the Eulerian and Lagrangian models as well as the experimental data. The fourth case was person-to-person particle transport in the first-class cabin of an MD-82 aircraft cabin with heated manikins, from Chen et al. (2013). Experimental data as well as the results from Eulerian and Lagrangian models were used to assess the performance of the Markov chain model in a realistic scenario of airborne infectious disease transmission.

3.1 Case 1: Particle transport from a single pulsed source

The first case was that of particle transport from a single pulsed source in an empty chamber. Figure 1 shows the configuration of the chamber studied by Wang and Chen (2009). The dimensions of the chamber were $2.44 \times 2.44 \times 2.44$ m^3. An isothermal jet from an inlet at the upper edge of the chamber developed along the ceiling and then moved downward, forming a circulation pattern in the chamber. This is a basic forced convection airflow pattern in a mechanically ventilated room. The air change rate was 22.6 ACH. The thermo-fluid boundary conditions were measured by Wang and Chen (2009). Our study modeled a scenario with a pulsed source near the inlet, and another scenario with a pulsed source in the circulation zone. Particle transport in the first scenario was dominated by convection, while turbulent diffusion

also served as an important driven force in the second scenario. In the scenario with the pulsed source, the duration of the particle source was one time step.

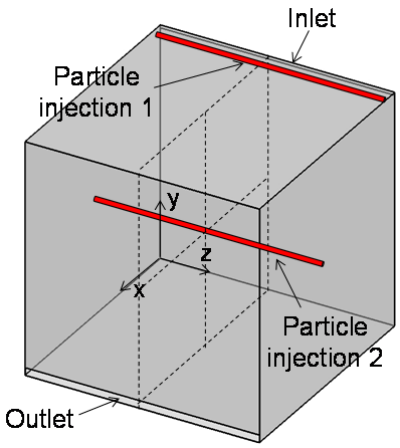

Figure 1. Configuration of the empty chamber studied by Wang and Chen (2009).

Three structured grid resolutions (8,000, 51,840, and 414,720) were tested for CFD grid independence. The resolution of 51,840 was sufficiently fine to produce accurate results for the airflow in the chamber. The Markov chain, Eulerian, and Lagrangian models were used to calculate transient particle transport. The particle diameter and density used was 1 μm and 1000 kg/m^3, respectively. Particle deposition and resuspension were neglected because of their limited effects (Zhao et al., 2009; Zhu et al., 2012). Therefore, for the Markov chain model, it was assumed that the probability of a particle moving from a near wall cell to the wall was zero. For the Eulerian model, it was assumed that the particle flux to/from the wall was zero. For the Lagrangian model, the "reflect" type of boundary condition was used, which means that, when reaching a wall, the particle rebounded without losing its momentum. Such treatments were also applied for the other cases. Furthermore, for the Lagrangian model, the necessary particle number injected from the source was 1.61 million according to Eq. (20). For all the three models, the time step size should be small enough to capture the transient features of particle transport. Theoretically, the transient features can be fully captured if, in each time step, the particles move across a distance that is less than the width of a cell, i.e., the Courant number is less than 1 (Courant et al., 1928). Therefore, a suitable time step size can be estimated by the following equation (Courant et al., 1928):

$$\Delta t \le \min(\frac{l}{u}) \tag{21}$$

where l is the distance between the centroids of two adjacent cells, and u is the air velocity at the connecting face of the two cells. The time step size was set at 0.01 s for this case according to Eq. (21). The time step sizes for the other cases were determined using the same method.

Figure 2 compares the transient particle concentration distributions at the plane of z=1.22 m predicted by the Markov chain, Eulerian, and Lagrangian models for the scenario with a pulsed source near the inlet. All the particle concentrations were normalized by the maximum concentration at the source. All three models predicted that the particles moved along the ceiling, traveled downward along the right wall, moved to the floor, and finally were dispersed throughout the whole chamber by means of recirculation. Figure 3 compares the

three models for the scenario with a pulsed source in the circulation zone at the plane of z=1.22 m. For these two scenarios, the Markov chain model agreed well with the Eulerian and Lagrangian models in terms of the general trend of transient particle transport in the chamber.

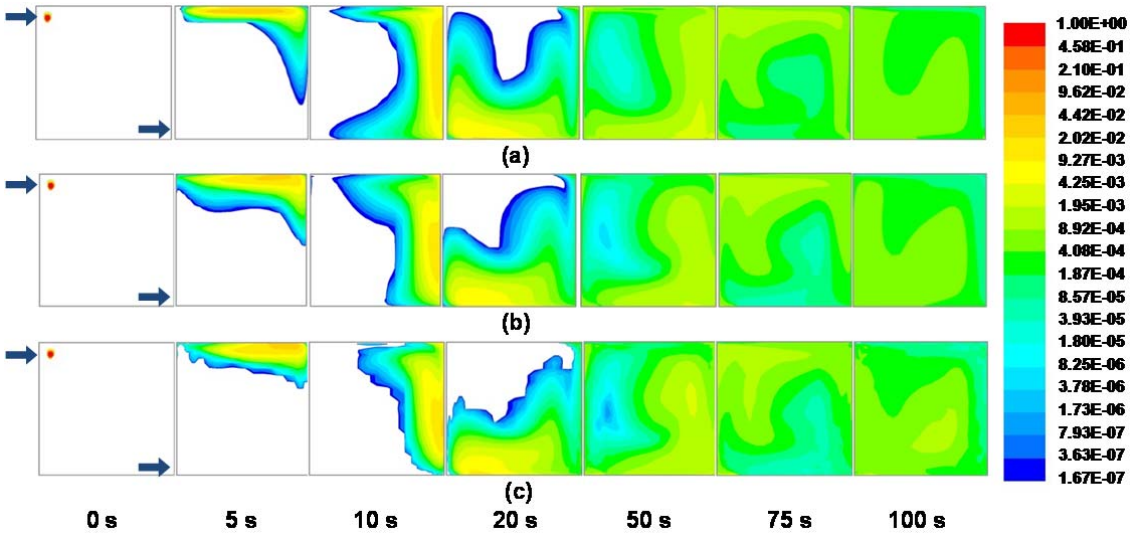

Figure 2. Comparison of normalized particle concentration distributions at the plane of z=1.22 m with a pulsed source near the inlet predicted by (a) the Markov chain model, (b) the Eulerian model, and (c) the Lagrangian model.

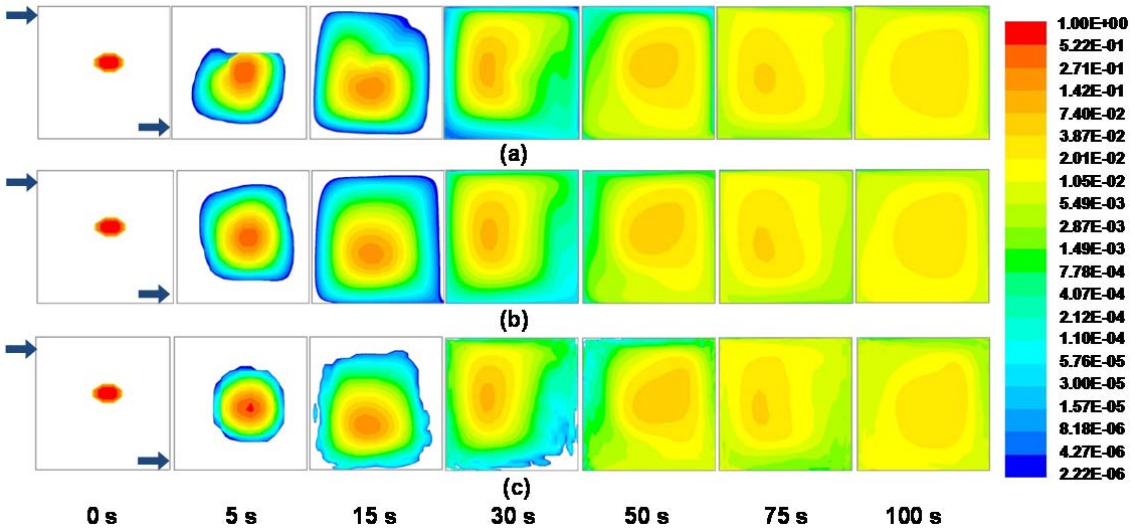

Figure 3. Comparison of normalized particle concentration distributions at the plane of z=1.22 m with a pulsed source in the circulation zone predicted by (a) the Markov chain model, (b) the Eulerian model, and (c) the Lagrangian model.

3.2 Case 2: Particle transport from a source at the inlet

The second case was that of transient particle transport from a source at the inlet in an isothermal ventilated chamber, as studied by Zhang et al. (2009). The dimensions of the chamber were 4 m in length, 2.1 m in width, and 2.4 m in height, as shown in Figure 4. The averaged air velocity and incident angle of the supply air were 0.84 m/s and 10° downward,

respectively. Particles with a size of 1 μm were injected through the inlet into the chamber. The particle density was 1000 kg/m^3. Particle concentrations as a function of time were measured at two locations. The two measurement locations (Point 1 and Point 2) were 1.8 and 0.9 m, respectively, from the floor, as shown in Figure 4. Zhang et al. (2009) used two optical particle counters to measure the particle concentrations at one of the measurement locations and the inlet simultaneously. Thus, two independent experiments were conducted in order to obtain the results at the two locations.

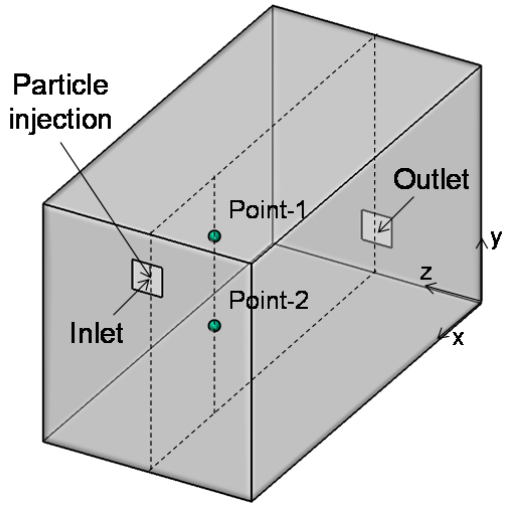

Figure 4. Configuration of the chamber studied by Zhang et al. (2009).

This study used a grid resolution of 18,009, which was sufficiently fine to produce accurate results for the airflow in the chamber (Chen et al., 2015a). The Markov chain, Eulerian, and Lagrangian models were used to calculate the transient particle concentration distributions. The time step size was set at 0.01 s according to Eq. (21). Particle deposition and resuspension were negligible at a particle size of 1 μm (Zhao et al., 2009; Zhu et al., 2012). It should be noted that two sets of simulations were performed on the basis of the corresponding inlet particle concentrations, as shown in Figure 5. For the Lagrangian model, the necessary particle number injected from the source was 2.24 million according to Eq. (20).

Figure 5 compares the numerical results for transient particle concentration as predicted by the Markov chain, Eulerian, and Lagrangian models and as measured experimentally. Figure 5(a) compares the results at the location with a height of 1.8 m. It can be seen that the simulations at this location show particle concentration profiles that are similar to that at the inlet, which all had a strong peak at the beginning. This similarity occurred because this location was close to the inlet. All three models correctly predicted the peak in particle concentration in the initial stage that was observed in the experimental data. However, as shown in Figure 5(b), both the simulations and the experiment exhibited a smaller peak than that in Figure 5(a). Furthermore, all three models captured the fact that the peak was delayed in time at this location. This weaker response was due to the greater distance between this location and the source. Note that the transport of fine particles is mainly determined by the airflow distribution (Chen and Zhao, 2010). Therefore, the discrepancies between the experimental data and numerical results may be mainly attributed to the differences between the measured and calculated airflow field. Furthermore, the discrepancies may be partially attributed to the heat generation by the particle counters and its associated convective flows.

Generally speaking, the Markov chain model predicted the trends in transient particle concentration with similar accuracy to the Eulerian and Lagrangian models.

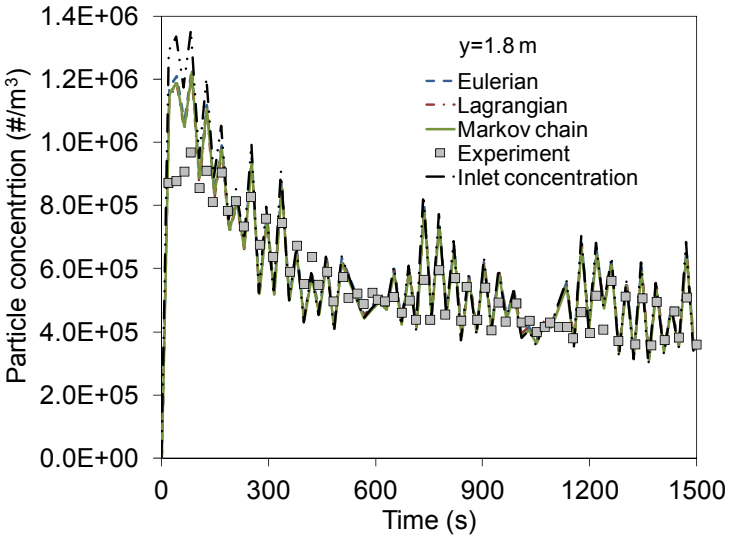

(a)

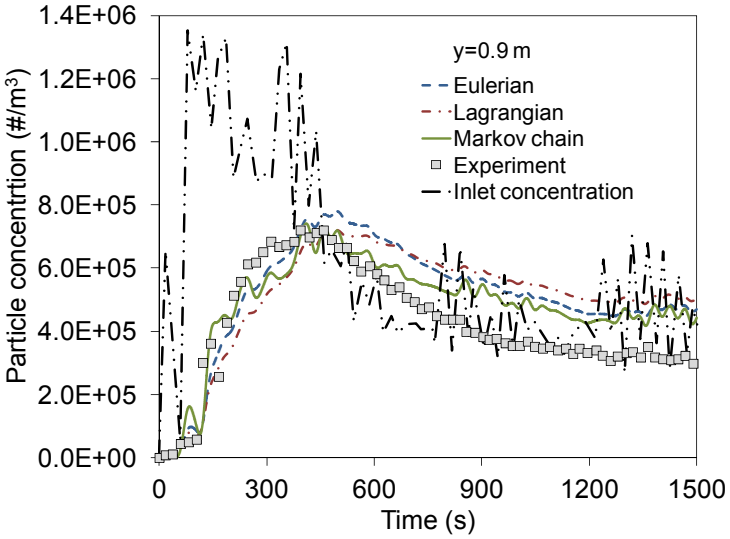

(b)

Figure 5. Comparison of the numerical results for transient particle concentration predicted by the Markov chain, Eulerian, and Lagrangian models with the corresponding experimental data at positions (a) y = 1.8 m and (b) y = 0.9 m.

3.3 Case 3: Particle transport from a source inside the chamber

The third case was that of particle transport from a source inside a chamber with displacement ventilation, as shown in Figure 6 (Bolster and Linden, 2009). The chamber dimensions were 2.6 m in length, 1.3 m in width, and 1.8 m in height. The air was supplied through four linear slot diffusers around the floor, and the exhausts were located at ceiling level. The air velocity at the supply inlet was 0.08 m/s. There was a heated box with a power of 65 W on the floor. The particle source was located above the box. The particle size was 2 μm, The particle density was 1000 kg/m^3, and the duration of particle release was 328 s. Transient particle concentrations were measured at five locations, which were 0.2, 0.6, 1.1, 1.4, and 1.7 m above the floor, respectively, as shown in Figure 6.

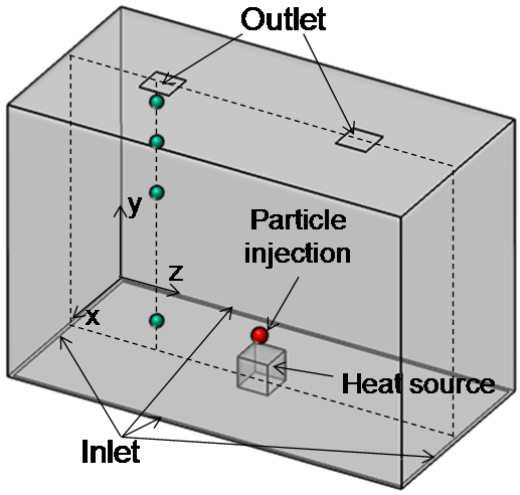

Figure 6. Configuration of the chamber studied by Bolster and Linden (2009).

Our study used a grid resolution of 53,740, which was sufficiently fine (Chen et al., 2015a). The Markov chain, Eulerian, and Lagrangian models were used to calculate the particle concentration as a function of time. The time step size was set at 0.01 s according to Eq. (21). This study neglected particle deposition and resuspension for this case (Zhao et al., 2009; Zhu et al., 2012). For the Lagrangian model, the necessary particle number injected from the source was 0.68 million according to Eq. (20).

Figure 7 compares the numerical results for transient particle concentration as predicted by the Markov chain, Eulerian, and Lagrangian models and as measured experimentally. This investigation normalized all the particle concentrations by the maximum concentration at the location with a height of 1.7 m. At the locations with heights of 1.7 and 1.4 m, the three models obtained particle concentration profiles that were similar to the experimental data. At the location with a height of 1.1 m, the peak in particle concentration in the experimental data was delayed as compared with the peak at the 1.7 and 1.4 m locations, and this delay was correctly captured by all the models. In addition, all three models correctly predicted extremely low particle concentrations at the locations with heights of 0.6 and 0.2 m. To keep this paper concise, the results at these two locations are not presented here. Again, the discrepancies between the experimental data and calculated results may be mainly attributed to the differences between the modeled and measured airflow field. In general, the Markov chain model again predicted the trends in transient particle transport with similar accuracy to the Eulerian and Lagrangian models.

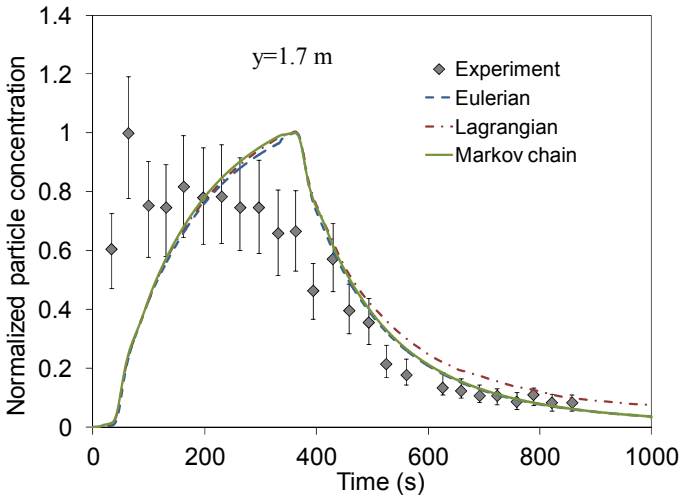

(a)

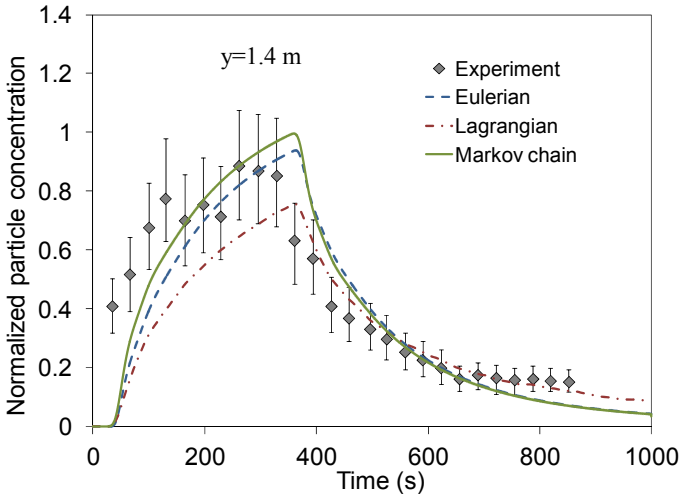

(b)

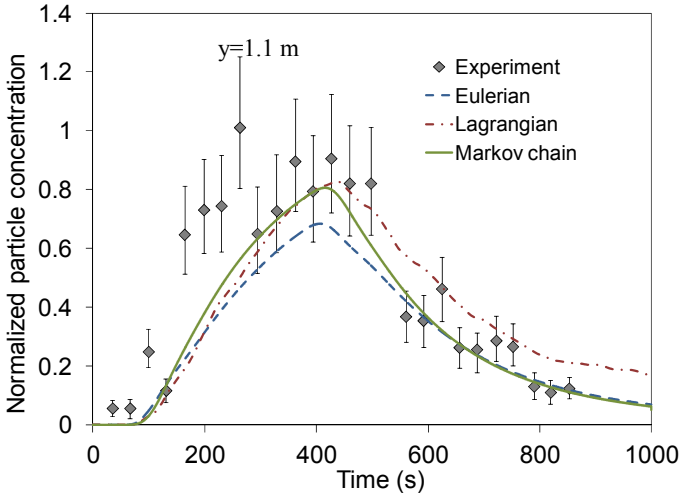

(c)

Figure 7. Comparison of the numerical results for transient particle concentration predicted by the Markov chain, Eulerian, and Lagrangian models with the corresponding experimental data at three positions: (a) y = 1.7 m, (b) y = 1.4 m, and (c) y = 1.1 m.

3.4 Case 4: Person-to-person particle transport in an airplane

The fourth case was that of person-to-person particle transport in the first-class cabin of an MD-82 airplane, as shown in Figure 8. Liu et al. (2012) have described the aircraft cabin and measured the thermo-fluid boundary conditions in detail. The cabin contained three rows with a total of 12 seats as numbered in Figure 8. The cabin was fully occupied by heated manikins. Particles with a diameter of 3 μm were released into the cabin from the mouth of the manikin in Seat 2C for duration of 20 s. The particle density was 912 kg/m^3. The particle concentration as a function of time was measured at the breathing zone of each passenger. Detailed information about the experiment is provided by Chen et al. (2013).

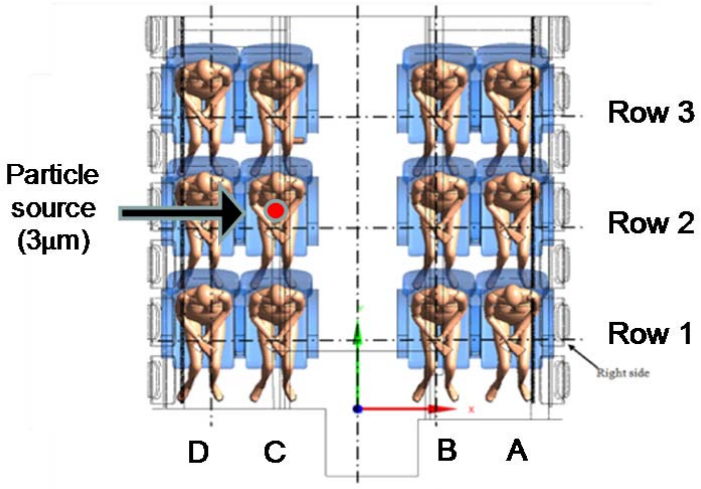

Figure 8. Schematic of the fully occupied first-class cabin: plane view (Chen et al., 2013).

In the simulation, this investigation used grid points equal to 6.4 million, which has been proven to be sufficiently fine (Chen et al., 2013). The Markov chain, Eulerian, and Lagrangian models were used to calculate the transient particle concentration distributions. The time step was set at 0.01 s according to Eq. (21). Particle deposition and resuspension at a particle size of 3 μm were negligible (Chen et al., 2013). For the Lagrangian model, the necessary particle number injected from the source was 1.76 million according to Eq. (20).

Figure 9 compares the normalized particle concentration distribution as a function of time as predicted by the Markov chain, Eulerian, and Lagrangian models and as measured experimentally. Chen et al. (2013) showed that the particle concentrations at Seats 1B and 1C were relatively high, while those at the other seats were relatively low. Figures 9(a) and 9(b) show that all three models accurately predicted the relatively high peak concentrations at Seats 1B and 1C that were observed in the experimental data. For the other seats, where the concentrations were relatively low, the comparison results are shown only for Seats 2B and 3B in Figures 9(c) and 9(d), respectively, in order to keep the paper concise. Seat 3B is representative of the locations at which the agreement between the simulation and experiment was very good, while Seat 2B is representative of those locations at which the agreement was worse. As shown in Figure 13 of Chen et al. (2013), the modeled and measured airflow field did not match well, which may be a main reason for the discrepancies between the experimental data and numerical results of particle transport. Generally speaking, the Markov chain model can provide the transient particle concentration distribution with similar

accuracy to the Eulerian and Lagrangian models for such a complex case.

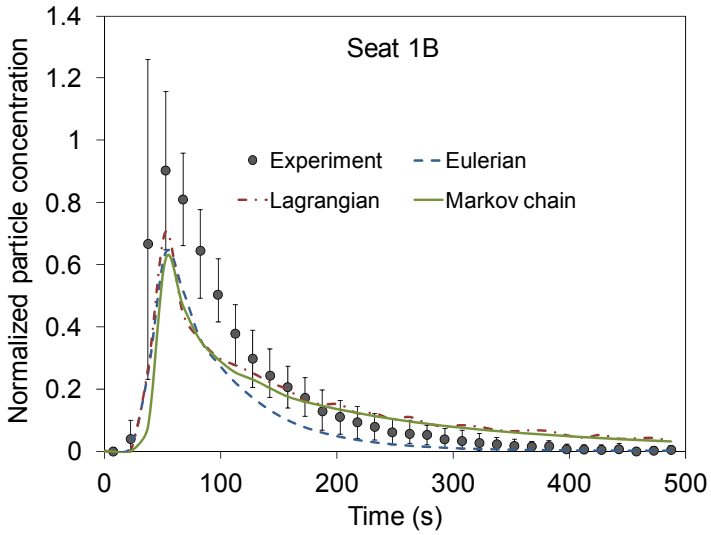

(a)

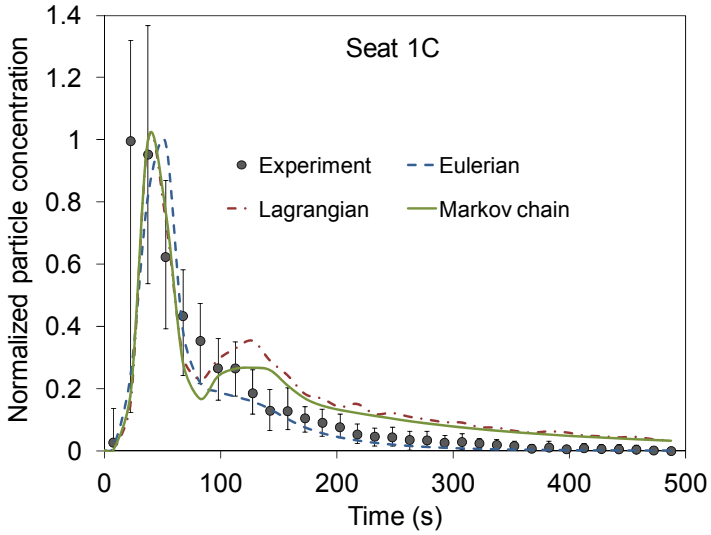

(b)

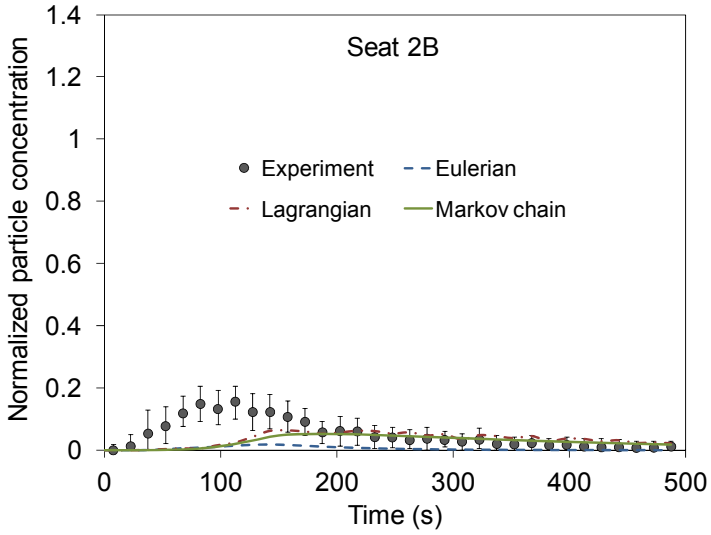

(c)

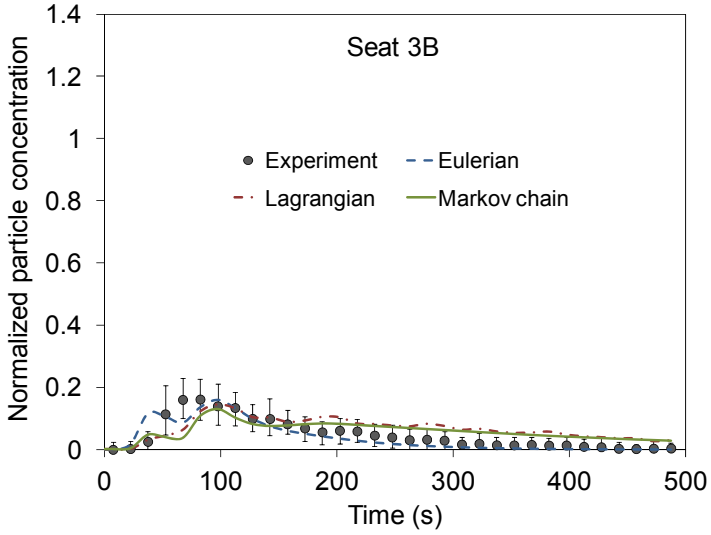

(d)

Figure 9. Comparison of the numerical results for transient particle concentration predicted by the Markov chain, Eulerian, and Lagrangian models with the corresponding experimental data at seats (a) 1B, (b) 1C, (c) 2B, and (d) 3B.

3.5 Quantitative comparison of the accuracy

This study used two indexes, correlation coefficient (R) and normalized root-mean-square deviation (NRMSD), to quantitatively compare the accuracy of each model. The correlation coefficient between the experimental data and modeling results was calculated by:

$$R = \frac{\sum_{i=1}^{n}(C_{\text{exp},i} - \overline{C_{\text{exp}}})(C_{\text{model},i} - \overline{C_{\text{model}}})}{\sqrt{\sum_{i=1}^{n}(C_{\text{exp},i} - \overline{C_{\text{exp}}})^2 \sum_{i=1}^{n}(C_{\text{model},i} - \overline{C_{\text{model}}})^2}} \tag{22}$$

where $C_{\text{exp,i}}$ is a data point from the experimental data, and $C_{\text{model,i}}$ is the corresponding data

point from the modeling results. $\overline{C_{\text{exp}}}$ and $\overline{C_{\text{model}}}$ represents the average value of the experimental data and the corresponding modeling results, respectively. The normalized root-mean-square deviation was calculated by:

$$NRMSD = \frac{\sqrt{(\sum_{i=1}^{n}(C_{\text{exp},i} - C_{\text{model},i})^2)/n}}{C_{\text{exp,max}} - C_{\text{exp,min}}} \tag{23}$$

where $C_{exp,max}$ and $C_{exp,min}$ is the maximum and minimum value of experimental data, respectively.

Table 1 lists the calculated correlation coefficients and normalized root-mean-square deviations between the experimental data and modeling results for Cases 2 to 4. Since the experimental data of particle concentration was not available for Case 1, the results for this case cannot be obtained. As shown in Table 1, the correlation coefficients and normalized root-mean-square deviations between experimental data and modeling results were rather comparable among the three models for Cases 2 to 4. Therefore, it can be concluded that the Markov chain model can provide the transient particle concentration distribution with similar accuracy to the Eulerian and Lagrangian models.

Table 1. Correlation coefficients (R) and normalized root-mean-square deviations (NRMSD) between experimental data and modeling results for the three models.

Case No.	R			NRMSD		
	Markov chain	Eulerian	Lagrangian	Markov chain	Eulerian	Lagrangian
2	0.90	0.89	0.83	0.10	0.11	0.13
3	0.90	0.87	0.84	0.14	0.15	0.17
4	0.68	0.74	0.68	0.10	0.09	0.10

4. Comparison of computing costs for the three models

The comparisons above show that the Markov chain model can provide information about transient particle transport with similar accuracy to the Eulerian and Lagrangian models. Computing cost is another important factor in the identification of an efficient model. This section evaluates the computing cost of the Markov chain model by comparing it with the Eulerian and Lagrangian models. Note that the comparison was on the basis of using the same time step size, determined according to Eq. (21), in all three models. The influence of time step size will be discussed in section 5.1.

Theoretically, the computing cost of Markov chain model, which does not require any iterations, is related only to the grid number. For the Eulerian model, the computing cost is related to the grid number as well as the number of iterations in each time step. For the Lagrangian model, the cost factors include the grid number and the number of particles being tracked. The necessary particle number for the Lagrangian model can be calculated by Eq. (18). It can be seen that the particle source duration can influence the necessary particle number and therefore the computing time. To isolate the impact of source duration, this study substituted the combined Lagrangian and superimposition method for the pure Lagrangian

method. With the combined method, the necessary particle number can be calculated by Eq. (20), which is independent from the source duration. For the purpose of a fair comparison among the cases, the ratio of V_{room} to V_{target} was set at a consistent value of 1000, so that the number of particles being tracked was the same for all cases. A ratio of 1000 ensured that the volumes of the target zones were of the same magnitude in all three cases, and that they were smaller than the volumes of the breathing zones. This investigation first used these assumptions to fairly compare the computing costs and to develop empirical equations for determining the relative computing times of the three models. Next, the empirical equations were modified to account for the effects of source duration and the ratio of V_{room} to V_{target} with the Lagrangian model. Furthermore, for the purpose of a faircomparison, all the cases were calculated over a period of five time constants of the room, 5τ (Eq. (19)), and the time step size was set at the same value for all models.

To quantitatively investigate the speed of calculation, this study determined the relative computing times of the three models. For each case, the computing time of the Eulerian model relative to that of the Markov chain model was defined as:

$$\eta_{E/M,i} = \frac{t_{Eulerian,i}}{t_{Markov,i}} \tag{23}$$

where $t_{Eulerian,i}$ and $t_{Markov,i}$ are the computing times of the Eulerian and Markov chain models, respectively, for Case i. Similarly, the computing time of Lagrangian model relative to that of the Markov chain model was defined as:

$$\eta_{L/M,i} = \frac{t_{Lagrangian,i}}{t_{Markov,i}} \tag{24}$$

where $t_{Lagrangian,i}$ is the computing time of the Lagrangian model for Case i.

Figure 10 shows the relative computing times for the four cases as a function of grid number. The linear regression shows that the computing time of the Eulerian model relative to that of the Markov chain model was independent of the grid number (the slope was zero). This occurred because the only difference between the Eulerian and Markov chain models in regard to computing time was the number of iterations in each time step. Normally, the Eulerian model requires several iterations in each time step, while the Markov chain model does not require any iterations. For a given grid number, the computing time of the Eulerian model for a single iteration is comparable to that of the Markov chain model for a single time step. Therefore, the computing time of the Eulerian model relative to that of the Markov chain model depends only on the number of iterations required by the Eulerian model in each time step. For the studied cases, on average, the Eulerian model required five to six iterations in each time step, where the simulations were assumed to have converged when the residual for the particle equation was less than 1×10^{-5}. Therefore, according to regression analysis, the computing time of the Eulerian model relative to that of the Markov chain model is:

$$\eta_{E/M,i} = \frac{t_{Eulerian,i}}{t_{Markov,i}} = 5.59 \tag{25}$$

The factor of reduction in computing time may change if a different number of iterations is

used.

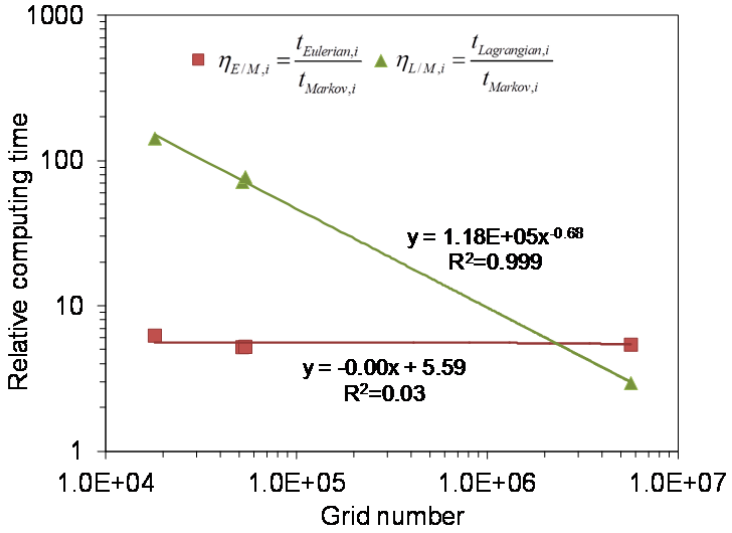

Figure 10. Relative computing time as a function of grid number for the Markov chain, Eulerian, and Lagrangian models.

Figure 10 also shows that the computing time of the Lagrangian model relative to that of the Markov chain model was negatively associated with the grid number. When the grid number was relatively small, the Lagrangian model required a much longer computing time than did the Eulerian and Markov chain models. However, when the grid number was relatively large, the Lagrangian model required less computing time than the other two models. As indicated in Eq. (15), the calculation of particle trajectory is independent of the grid number. Therefore, the influence of grid number on the computing time of the Lagrangian model tends to be weaker than its influence on the other two models. As shown in the figure, a power function could satisfyingly describe the relationship between the relative computing time of the Lagrangian to Markov chain model and the grid number:

$$\eta_{L/M,i} = \frac{t_{Lagrangian,i}}{t_{Markov,i}} = 1.18\times10^{5}\cdot n^{-0.68} \tag{26}$$

where n is the grid number. It should be noted that this equation was based on the assumption that the ratio of V_{room} to V_{target} was equal to 1000. To account for the impact of this ratio, Eq. (26) should be modified as:

$$\eta_{L/M,i} = \frac{t_{Lagrangian,i}}{t_{Markov,i}} = 1.18\times10^{5}\cdot n^{-0.68}\cdot\frac{V_{\text{room}}}{1000\cdot V_{\text{target}}} = 118\cdot n^{-0.68}\cdot\frac{V_{\text{room}}}{V_{\text{target}}} \tag{27}$$

Moreover, the above equation was developed on the basis of the combined Lagrangian and superimposition method in order to isolate the impact of source duration. If the pure Lagrangian method was used, the necessary particle number would be increased by a factor that can be expressed as (Chen et al., 2015b):

$$\frac{N_{\text{nec}}}{N_{\text{nec,sup}}} = \frac{\frac{t_s}{\tau}}{1-\exp(-\frac{t_s}{\tau})} \tag{28}$$

Therefore, to account for the impact of source duration, Eq. (28) should be further modified as:

$$\eta_{L/M,i} = \frac{t_{Lagrangian,i}}{t_{Markov,i}} = 118 \cdot n^{-0.68} \cdot \frac{V_{\text{room}}}{V_{\text{target}}} \cdot \frac{\frac{t_s}{\tau}}{1-\exp(-\frac{t_s}{\tau})} \tag{29}$$

Empirical equations (25) and (29) can be used to evaluate the relative computing time of the Markov chain, Eulerian, and Lagrangain models. They can together serve as a general guideline for selecting an efficient model to calculate transient particle transport in indoor environments.

5. Comparison of the robustness of the three models

5.1 Influence of time step size

In the above comparison of the Markov chain, Eulerian, and Lagrangian models, the same time step size, chosen according to Eq. (21), was used in all three models. The chosen time step sizes were small enough to fully capture the transient features of particle transport in every cell of the domain, because the Courant number was less than 1. However, for engineering applications, modelers normally are concerned about the transient feature of particle transport only in certain locations, such as breathing zones. In this case, if the particle concentration does not change rapidly in these locations, the time step size may be set at a larger value in order to reduce the computing cost. This section reports our effort in exploring the influence of time step size on transient particle transport prediction with the three models.

This study conducted a sensitivity analysis of time step size using the Markov chain, Eulerian, and Lagrangian models for Case 2. The original time step size was set at 0.01 s, according to Eq. (21). Two larger values, 0.05 and 0.5 s, were also tested. Figure 11 compares the transient particle concentrations predicted by the three models with time step sizes of 0.01, 0.05, and 0.5 s. For the Eulerian and Lagrangian models, the predicted results for the different time step sizes agree very well with one another. Thus, the transient particle concentrations were relatively insensitive to time step size for the Eulerian and Lagrangian models. However, for the Markov chain model, a larger time step size resulted in lower particle concentrations. This difference occurred because, according to Eq. (2), the particles can move only to the adjacent cells in a time step. When the time step size was too large, the Markov chain model was not able to make the particles move beyond the adjacent cells. In this case, the transport of particles was slower than it would be in reality. Thus, the transient particle concentrations were highly sensitive to time step size for the Markov chain model.

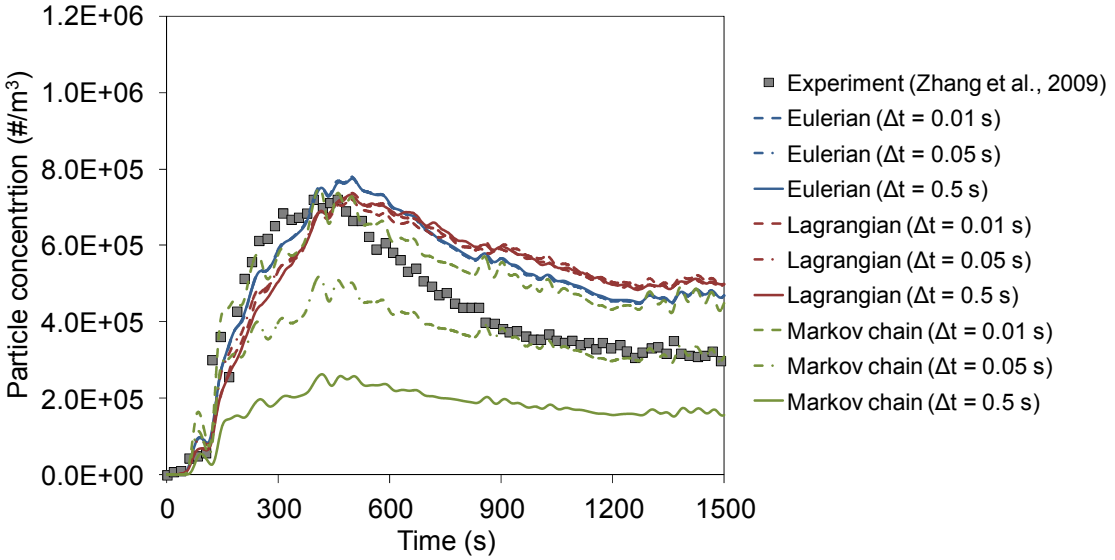

Figure 11. Comparison of transient particle concentrations predicted by the Markov chain, Eulerian, and Lagrangian models with time step sizes of 0.01, 0.05, and 0.5 s.

5.2 Other influencing factors

The Eulerian and Lagrangian models are mature and well-developed models for simulation of transient particle transport. Although the airflow in the cases above was steady-state, the Eulerian and Lagrangian models can also be used under unsteady-state airflow conditions (Wang et al., 2012). Furthermore, these two methods can account for other mechanisms of particle dispersion, such as gravitational settling and thermophoresis (Zhao et al., 2004; Zhao et al., 2009), as well as particle deposition onto surfaces (Chen et al., 2006; Zhao et al., 2009). On the other hand, the newly developed Markov chain model cannot account for the influencing factors mentioned above, and currently it can calculate the transient particle transport only from a single pulsed source. Another shortcoming of this model is the requirement of a small time step size. Nevertheless, the Markov chain model generally entails a far lower computing cost than do the other two models.

6. Discussion

This study compared the Markov chain model with the traditional Eulerian and Lagrangian models in terms of accuracy, computing cost, and robustness. All of the three models are physically plausible, so their accuracy is comparable, which has been confirmed by the cases studied in this paper. In terms of computing cost, with the same time step size and Courant number smaller than 1, the Markov chain model is about 6 times faster than the Eulerian model. For engineering applications of indoor environments, the grid number is normally in the order of 10^4 to 10^6. With such grid numbers, the Markov chain model can be about 10 to 100 times faster than the Lagrangian model. Therefore, when the particle deposition, resuspension, evaporation, biological and chemical reaction were negligible and the same time step size (Courant number $\leqslant 1$) is used, the Markov chain model is preferred because of its reasonable accuracy and low computing cost, followed by the Eulerian model, and then the Lagrangian model. However, the current version of Markov chain model has not yet been able to account for the influencing factors mentioned above. Therefore, when these factors become significant, the mature and well-developed Eulerian and Lagrangian models are superior to the newly developed Markov chain model. Since the Markov chain model has the

potential to reduce computing cost, it is worthwhile to account for these influencing factors and implement more functions to the current version of Markov chain model in the future.

Furthermore, the time step size can significantly affect the speed of calculation and accuracy. The results from this study indicated the following remarks. When the transient features in every cell of the domain are of concern, the time step size should be small enough (Courant number $\leqslant$ 1) for all three models. In this case, the Markov chain model had the highest calculation speed among the three models without scarifying the accuracy. However, in some cases, only the transient features in certain cells where particle concentration does not change rapidly are of concern. When calculating such cases with a larger time step size (Courant number > 1), the Eulerian and Lagrangian models may be still able to provide accurate results in these cells, while the Markov chain model may not. To ensure the accuracy for these cells in such cases, modelers need to run the Markov chain model with a finer time step size when compared with the other two models, which increases the computing time. A possible solution would be merging the cells where particle concentration changes rapidly so that the time step size could be relaxed for Markov chain model, which deserves further study.

7. Conclusions

This investigation compared the Markov chain model with the Eulerian and Lagrangian models for use in indoor transient particle transport simulations. The models were compared on the basis of accuracy, computing cost, and robustness. The following conclusions can be made:

(1) The Markov chain model can predict transient particle transport in enclosed environments with similar accuracy to the Eulerian and Lagrangian models.
(2) When the same time step size (Courant number $\leqslant$ 1) and grid number were used for all three models, the Markov chain model was the fastest. Unless a super-fine grid was used, the Eulerian model was faster than the Lagrangian model.
(3) This study developed empirical equations to quantitatively evaluate the relative computing costs for the three models.
(4) Because the Markov chain model was sensitive to time step size when the Courant number is larger than 1, the Eulerian and Lagrangian models were more robust than the Markov chain model.

Acknowledgements

The research presented in this paper was partially supported by the National Basic Research Program of China (the 973 Program) through Grant No. 2012CB720100 from the Ministry of Science and Technology of China.

References

Aliabadi, A.A. and Rogak, S.N. (2011). Lagrangian stochastic particle tracking. Aerosol Sci. Tech., 45: 313-314.

ANSYS. (2010). Fluent 12.1 Documentation. Fluent Inc., Lebanon, NH.

Bolster, D.T. and Linden, P.F. (2009). Particle transport in low-energy ventilation systems. Part 2: Transients and experiments. Indoor Air, 19: 130-144.

Chao, C.Y.H. and Wan, M.P. (2006). A study of the dispersion of expiratory aerosols in unidirectional downward and ceiling-return type airflows using a multiphase approach. Indoor Air, 16: 296-312.

Chen, C. and Zhao, B. (2010). Some questions on dispersion of human exhaled droplets in ventilation room: answers from numerical investigation. Indoor Air, 20: 95-111.

Chen, C., Liu, W., Li, F., Lin, C.-H., Liu, J., Pei. J. and Chen, Q. (2013). A hybrid model for investigating transient particle transport in enclosed environments. Build. Environ., 62: 45-54.

Chen, C., Lin, C.-H., Jiang, Z. and Chen, Q. (2014). Simplified models for exhaled airflow from a cough with the mouth covered. Indoor Air, 24: 580-591.

Chen, C., Liu, W., Lin, C.-H. and Chen, Q. (2015a). A Markov chain model for predicting transient particle transport in enclosed environments. Build. Environ., 90: 30-36.

Chen, C., Liu, W., Lin, C.-H. and Chen, Q. (2015b). Accelerating the Lagrangian method for modeling transient particle transport in indoor environments. Aerosol Sci. Tech. 49: 351-361.

Chen, F., Yu, S.C.M. and Lai, A.C.K. (2006). Modeling particle distribution and deposition in indoor environments with a new drift-flux model. Atmos. Environ. 40: 357-367.

Chen, Q. (1995). Comparison of different k-ε models for indoor air flow computations. Numer. Heat Tr. B-Fund. 28: 353-369.

Choudhury, D. (1993). Introduction to the Renormalization Group Method and Turbulence Modeling, Canonsburg, Fluent Inc. Technical Memorandum TM-107.

Courant, R., Friedrichs, K. and Lewy, H. (1928). On the partial difference equations of mathematical physics. IBM J. Res. Develop., 11: 215-234.

Gao, N. and Niu, J. (2007). Modeling particle dispersion and deposition in indoor environments. Atmos. Environ., 41: 3862-3876.

Gao, N., He, Q. and Niu, J. (2012). Numerical study of the lock-up phenomenon of human exhaled droplets under a displacement ventilated room. Build. Simul., 5: 51-60.

Gupta, J.K., Lin, C.-H. and Chen, Q. (2011a). Transport of expiratory droplets in an aircraft cabin. Indoor Air, 21: 3-11.

Gupta, J.K., Lin, C.-H. and Chen, Q. (2011b). Inhalation of expiratory droplets in aircraft cabins. Indoor Air, 21: 341-350.

Hang, J., Li, Y. and Jin, R. (2014). The influence of human walking on the flow and airborne transmission in a six-bed isolation room: Tracer gas simulation. Build. Environ., 77: 119-134.

Hinds, W.C. (1999). Aerosol Technology: Properties, Behavior, and Measurement of Airborne Particles, 2nd edition. New York: Wiley.

Li, X., Niu, J. and Gao, N. (2011). Spatial distribution of human respiratory droplet residuals and exposure risk for the co-occupant under different ventilation methods. HVAC&R Res., 17: 432-445.

Li, X., Niu, J. and Gao, N. (2012). Co-occupant's exposure of expiratory droplets—Effects of mouth coverings. HVAC&R Res., 18: 575-587.

Li, Y., Leung, G.M., Tang, J.W., Yang, X., Chao, C., Lin, J.H., Lu, J.W., Nielsen, P.V., Niu, J.L., Qian, H., Sleigh, A.C., Su, H.J., Sundell, J., Wong, T.W. and Yuen, P.L. (2007). Role of ventilation in airborne transmission of infectious agents in the built environment – A multidisciplinary systematic review. Indoor Air, 17: 2-18.

Liu, W., Wen, J., Chao, J., Yin, W., Shen, C., Lai, D., Lin, C.-H., Liu, J., Sun, H. and Chen, Q. (2012). Accurate and high-resolution boundary conditions and flow fields in the first-class cabin of an MD-82 commercial airliner. Atmos. Environ., 56: 33-44.

Menzies, D., Fanning, A., Yuan, L. and FitzGerald, J.M. (2000). Hospital ventilation and risk for tuberculous infection in Canadian health care workers, Ann. Int. Med., 133: 779-789.

Morawska, L. (2006). Droplet fate in indoor environments, or can we prevent the spread of infection? Indoor Air, 16: 335-347.

Morsi, S.A. and Alexander, A.J. (1972). An investigation of particle trajectories in two-phase flow systems. J. Fluid Mech., 55: 193-208.

Moser, M.R., Bender, T.R., Margolis, H.S., Noble, G.R., Kendal, A.P. and Ritter, D.G. (1979). An outbreak of influenza aboard a commercial airliner, Am. J. Epi., 110: 1-6.

Nicas, M., Nazaroff, W.W. and Hubbard, A. (2005). Toward understanding the risk of secondary airborne infection: Emission of respirable pathogens. J. Occup. Environ. Hyg., 2: 143-154.

Occupational Safety & Health Administration (OSHA), (2014). Technical Manual. Section II: Chapter 1, Personal sampling for air contaminants. Available: https://www.osha.gov/dts/osta/otm/otm_ii/pdfs/otmii_chpt1_allinone.pdf [accessed Oct 17, 2014].

Olsen, S.J., Chang, H., Cheung, T.Y., Tang, A.F., Fisk, T.L., Ooi, S.P., Kuo, H., Jiang, D.D., Chen, K., Lando, J., Hsu, K., Chen, T. and Dowell, S.F. (2003). Transmission of the severe acute respiratory syndrome on aircraft, New Eng. J. Med., 349: 2416-2422.

Ross, S.M. (1996). Stochastic Processes, 2nd Edn. John Wiley & Sons, Inc.

Seepana, S. and Lai, A.C.K. (2012). Experimental and numerical investigation of interpersonal exposure of sneezing in full-scale chamber. Aerosol Sci. Tech., 46: 485-493.

Student. (1908). The probable error of a mean. Biometrika 6: 1-25.

Wang, M. and Chen, Q. (2009). Assessment of various turbulence models for transitional flows in enclosed environment. HVAC&R Res., 15: 1099-1119.

Wang, M., Lin, C.-H. and Chen, Q. (2012). Advanced turbulence models for predicting particle transport in enclosed environment. Build. Environ., 47: 40-49.

Zhang, L. and Li, Y. (2012). Dispersion of coughed droplets in a fully-occupied high-speed rail cabin. Build. Environ., 47: 58-66.

Zhang, N., Zheng, Z., Eckels, S., Nadella, V.B. and Sun, X. (2009). Transient response of particle distribution in a chamber to transient particle injection. Part. Part. Syst. Charact., 26: 199-209.

Zhang, Z., Zhai, Z.Q., Zhang, W. and Chen, Q. (2007). Evaluation of various turbulence models in predicting airflow and turbulence in enclosed environments by CFD: Part 2 - comparison with experimental data from literature. HVAC&R Res., 13: 871-886.

Zhao, B., Chen, C. and Tan, Z. (2009). Modeling of ultrafine particle dispersion in indoor environments with an improved drift flux model. J. Aerosol Sci., 40: 29-43.

Zhao, B., Zhang, Y., Li, X., Yang, X. and Huang, D. (2004). Comparison of indoor aerosol particle concentration and deposition in different ventilated rooms by numerical method. Build. Environ., 39: 1-8.

Zhu, Y., Zhao, B., Zhou, B. and Tan, Z. (2012). A particle resuspension model in ventilation ducts. Aerosol Sci. Technol., 46: 222-235.